Investigation of synchroniser engagement in dual clutch transmission equipped powertrains

Abstract

Transient response of a dual clutch transmission (DCT) powertrain to synchroniser mechanism engagements is investigated using a lumped inertia model of the powertrain. Original research integrates lumped inertia powertrain models for the DCT with a detailed synchroniser mechanism model and two separate engine models, comprising of a mean torque model and a harmonic torque model, using torque derived from piston firing. Simulations are used to investigate the synchroniser mechanism engagement process in a previously unscrutinised operating environment. Simulations are performed using both engine torque models, with the mean torque model demonstrates the highly nonlinear nature of synchroniser mechanism engagement, and the powertrain response to the engagement process. Through the introduction of harmonic engine torques, additional excitation is present in the mechanism during engagement, and increased vibration of the synchroniser sleeve results. The impact of vibrations is particularly important to the increased wear of indexing chamfer contact surfaces.

Keywords: Synchroniser; “dual clutch transmission”; “engine torque”; powertrain

1. Introduction and background

The integral design and operation of dual clutch transmissions exposes synchroniser mechanisms to new sources of vibration during actuation. Traditional manual

transmissions release the clutch before synchronisation begins, isolating the synchroniser from forced engine vibration. Whereas, in DCTs, synchronisers are engaged with the engine still driving the vehicle through the alternate clutch, thus torsional vibrations generated in the engine can now be transmitted to the synchroniser during actuation, exposing it to increased wear and potentially causing failure of the mechanism through premature release of the ring as a result of vibration. Current synchroniser mechanism studies [1-4] focus on the impact of mechanism engagement on the driver or investigation of design and operational variables on the engagement process, analysing "double bump" phenomena and variation in chamfer alignments on engagement for manual transmissions.

Reliance of synchronisers on torque balancing and its highly nonlinear engagement process make the application of the mechanism in DCTs potentially problematic [5-6]. The unique design and control of DCTs actuates the synchroniser with the engine still driving the powertrain, engagement is no longer masked by the torque hole as is performed in manual transmissions. Indeed it is now exposed to aggressive loading during engagement, including the introduction of forced vibration from the engine and vehicle acceleration. Socin and Walters [6] suggest that exposure to excessive vibrations can lead to additional wear of friction surfaces, including chamfer and cone friction surfaces, or even premature unblocking of synchroniser mechanisms. Invariably detailed evaluation of the impact of the mechanism response in powertrains is ignored, with limited modelling detail of the powertrain for synchroniser studies [5].

The application of torsional lumped mass models to is a convenient method to investigate vehicle powertrains, examples for automatic transmission (AT) [7, 8] and dual clutch transmissions [9, 10] are available. Indeed such methods have become very effective tools for targeting specific focal points of research. Examples being Crowther's [7] analysis of backlash in AT transients or Kirschstein's [10] demonstrating of the influence of controller design for DCT vehicle launch. The most detailed model of DCT powertrains is presented by Goetz [11] for a front wheel drive powertrain, with the synchroniser is treated as a simple cone clutch for matching speeds, however other aspects of the engagement process, such as ring unblocking and hub indexing, are ignored. It is more popular to treat the synchroniser as a simple power switch [12] or ignore it completely [10]. Lumped parameter models can therefore provide useful insight powertrain transients resulting from synchroniser engagement for DCTs.

An important aspect of DCTs is that the engine now directly drives the transmission, it is not isolated from the powertrain as is found in conventional automatics. The use of mean engine torque models, such as Goetz [11] with an empirical model from Ref. [12] or torque map in Kulkarni [13], are useful for control but do not demonstrate effects of engine torque harmonics on the powertrain, as techniques provide the only mean output torque for the engine. In this paper both mean engine models and harmonic torque models are studied for synchroniser engagements. Mean torque models are used for identifying internal vibration of the powertrain generated during synchronisation and compared to transient response of synchroniser engagement with engine harmonics.

This paper therefore presents original research on the response of DCT equipped powertrains to synchroniser mechanism engagement process with and without engine harmonic induced vibration. In the following sections the development of a synchroniser mechanism model for nonlinear torques is presented in Section 2, followed by a thorough powertrain model with applied engine and vehicle resistance torques in Section 3. Damped free vibration analysis is performed in Section 4 to identify the system natural frequencies and damping ratios. The powertrain model is then used in transient simulations of synchroniser engagement in Section 5 with an mean torque and harmonic engine torques. This is used to compare the response of the powertrain to different engine models, and provide synchroniser dynamics during engagement. Further investigations of sleeve vibrations are performed using Fast Fourier Transforms in Section 6, before concluding remarks in Section 7.

2. Synchroniser mechanism dynamics and control

Synchroniser mechanism dynamics are governed by the torques generated in the cone clutch and chamfered splines, and to fully reveal these relationships this chapter is divided into three sub-sections. First the synchroniser mechanism is described and the process of engagement is defined. Second, the control apparatus is presented schematically and mathematical model discussed. Finally, the torques acting on the synchroniser mechanism and application as the control torque for modelling are defined, including procedure for modelling the sleeve motion during actuation.

2.1. Synchroniser mechanism and engagement process

The synchroniser comprises of three key elements that control the mechanism engagement, shown in Fig. 1. The sleeve, connected to the lay shaft via a splined saddle to enable axial translation only, receives actuation force from the actuator arm and hydraulic system to engage matching chamfers on both ring and hub. The ring comprises of external chamfered splines to mate with the sleeve and an internal cone clutch to engage the hub. The hub is mounted on the target gear and includes both the external cone clutch friction surface and indexing chamfers to engage the sleeve.

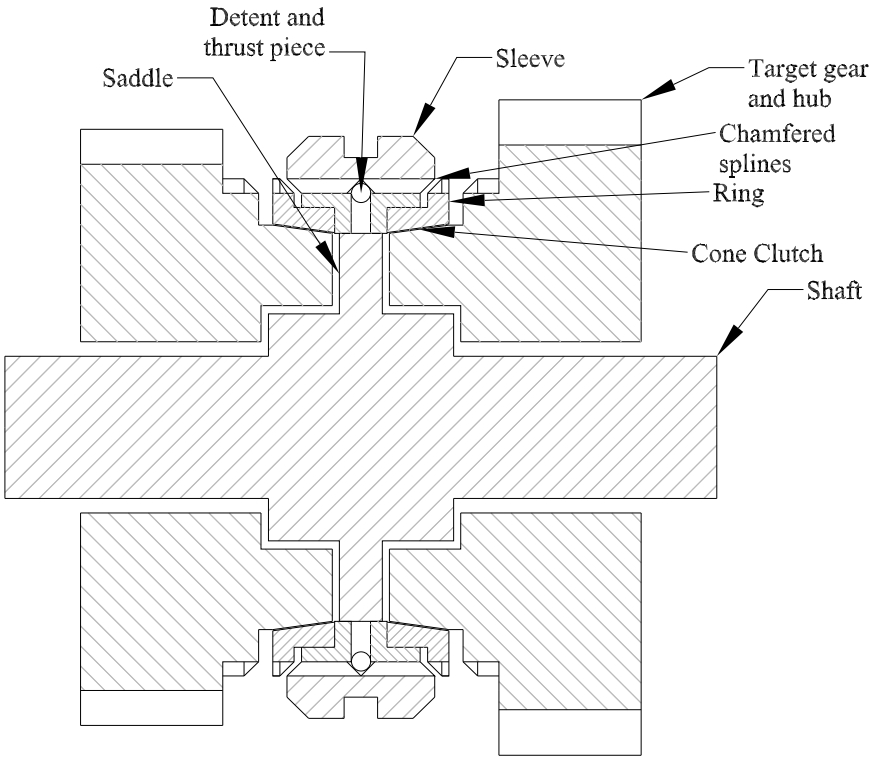

Figure 1: typical synchroniser mechanism cross-section

Synchronisation process begins with the sleeve seated in the neutral position, Fig. 2 (a), load is applied and the detents are breached. The sleeve pushes the ring forward and viscous torque in the cone clutch rotates the ring to the blocking position. Any oil film in

the cone is squeezed out as the ring moves forward until dry friction results in the cone. The ring is then rotated to block sleeve motion with chamfered splines on ring and sleeve in contact, speed synchronisation begins, Fig. 2 (b). This condition is maintained while cone clutch torque exceeds torque in blocking chamfers, typically to the completion of speed synchronisation. When blocking torque exceed the cone torque the ring is rotated by chamfer torque to the neutral position and sleeve passes over the ring to engage hub chamfers, initiating indexing, Fig. 2 (c). The final stage of the process is the realignment of sleeve and hub chamfers, where sleeve moves over the hub chamfer tips to interlock the target gear with the saddle completing engagement, Fig. 2 (d).

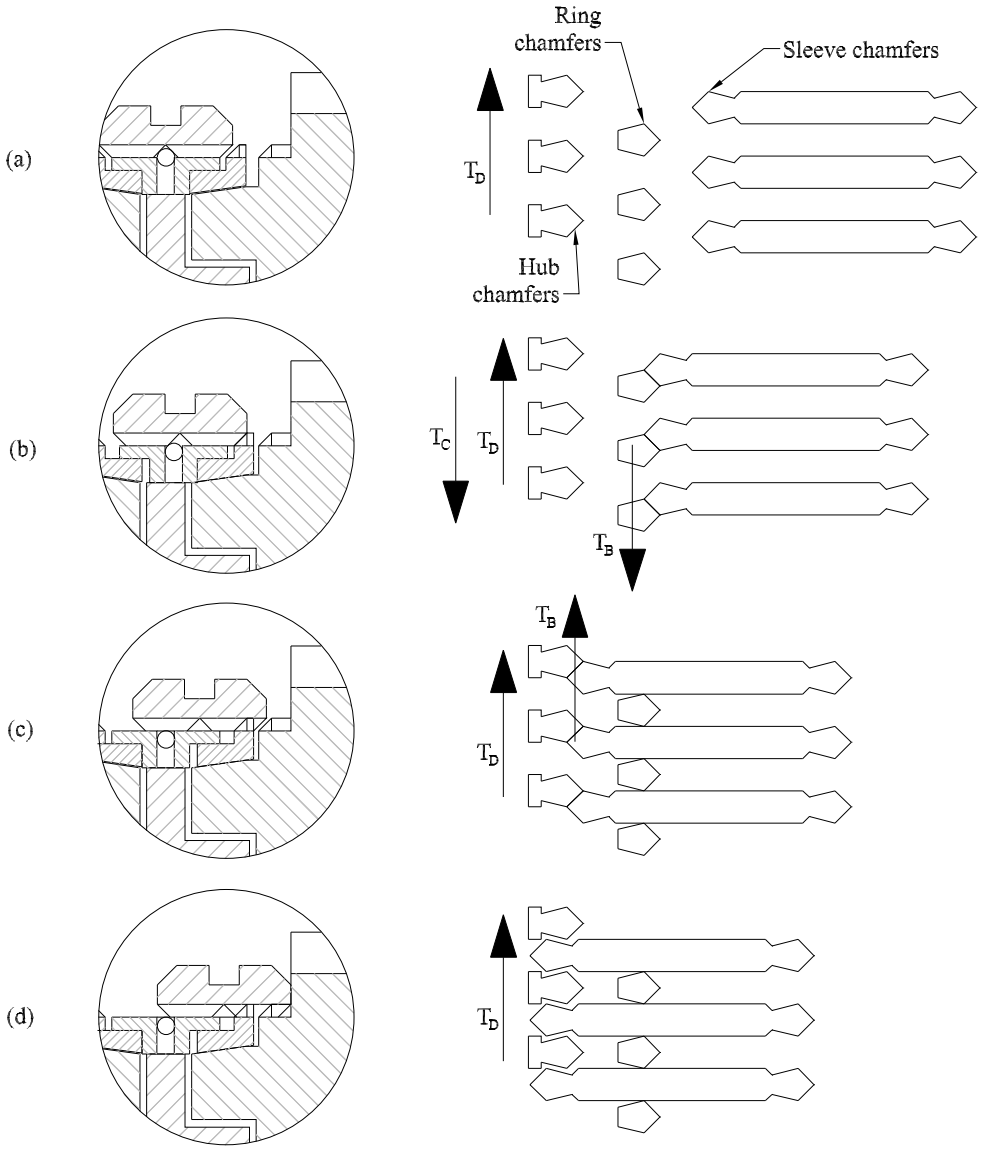

Figure 2: chamfer contact positions during separate steps of the synchronisation process, (a) sleeve in neutral position, (b) sleeve and ring in blocking position, (c) sleeve and hub in indexing position, and (d) sleeve interlocked with hub. T_D should be considered the net resistance torque acting on the synchroniser mechanism.

2.2. Hydraulic control system

The modelled hydraulic system consists of on/off solenoid simplified to a step pressure change with time delay of 50ms supplying a double acting cylinder arrangement pushing the mechanism forward to engage the synchroniser, shown in Fig. 3. The idle cylinder provides a resistant load to the engagement process, with excessive cylinder pressure inhibiting engagement.

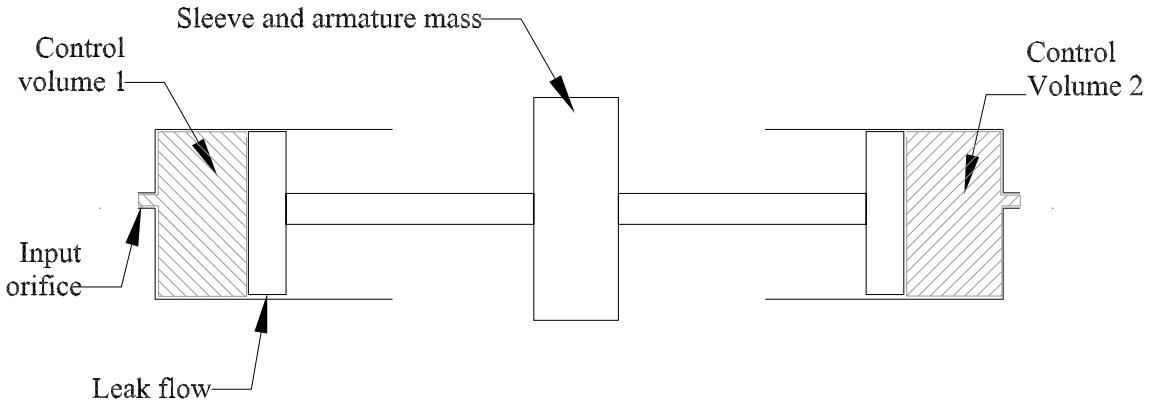

Figure 3: double acting cylinder model for the actuation of the synchroniser sleeve

The pressure for control volumes 1 and 2 is determined using the compressible fluid equation, with a bulk modulus of β = 1400GPa. The net flow into each chamber is calculated as input pressure from the control solenoid for active cylinder, $P_{syn} = 1.1e^{(-t/\tau)}$, and the exhaust pressure for the idle cylinder $P_{Exh} = 0.01$. Derivation of eqs. 1 and 2 can be found in Appendix 1, and are solved numerically to determine cylinder pressure.

$$P_{C1} = \int \frac{\beta}{V_0 + dV}\left(C_D \pi \frac{D_C{}^2}{4}\sqrt{P_{syn} - P_{C1}} - A_P \frac{dX_{syn}}{dt} - C_D \pi D_C c_r \sqrt{P_{C1} - P_{Exh}} \right) dt \qquad (1)$$

$$P_{C2} = \int \frac{\beta}{V_0 + dV}\left(C_D \pi \frac{D_C{}^2}{4}\sqrt{P_{Exh} - P_{C2}} + A_P \dot{X}_{syn} - C_D \pi D_C c_r \sqrt{P_{C2} - P_{Exh}} \right) dt \qquad (2)$$

Where τ signifies time delay, e is the exponent, P_{C1} is cylinder 1 pressure, P_{C2} is cylinder 2 pressure, β is bulk modulus, V_0 initial cylinder volume, dV change in cylinder volume, C_D is discharge coefficient, D_C is cylinder diameter, P_{syn} is control signal pressure, $\dot{X}_{syn}$ is sleeve velocity, P_{exh} is exhaust pressure, A_P is piston head area, and c_r is radial clearance.

With the sleeve controlled by the pressure loads from each of the two hydraulic cylinders, and given that any sleeve motion will encounter various sources of resistance during engagement, a general equation of motion for the sleeve is written, with F_R a general term for resistance forces, as:

$$m_S \ddot{x}_S = P_{C1} A_P - P_{C2} A_P - F_R \tag{3}$$

2.3. Synchroniser torque model

The torque generated by the synchroniser mechanism in the transmission is highly nonlinear, including a piecewise clutch model and chamfer torque defined as a function of sleeve location and relative orientation of blocking and indexing chamfers. To model the response of the ring – with very low inertia compared to the rest of the synchroniser – to the synchroniser torques would be numerically intensive without significantly improving results. Thus, the ring is removed from the dynamic model and replaced with a piecewise nonlinear torque model that comprises of the cone and chamfer torques, with variables of sleeve position and chamfer orientation used to define the output torque. The piecewise cone torque is:

$$T_C = \begin{cases} 4\pi\mu R_C^3 b \dfrac{\dot{\theta}_{syn}}{h} & X_S < X_0 \\ \dfrac{f_C F_S R_C}{\sin\alpha} & X_S \geq X_0, \dot{\theta} \neq 0 \\ T_{ST} & X_S \geq X_0, \dot{\theta} = 0 \\ \dfrac{f_{C,S} F_S R_C}{\sin\alpha} & X_S \geq X_0, \dot{\theta} = 0, T_{ST} > T_C \end{cases} \quad (4)$$

Where T_C is cone torque, X_S is the sleeve displacement, X_0 is the clearance between the sleeve neutral point and contact with ring chamfers, μ is lubricant viscosity, R_C is cone mean radius, $\dot{\theta}_{syn}$ is synchroniser slip speed, b is the half cone generatrix, h is cone separation, f_C is cone friction coefficient, F_S is sleeve force, α is cone angle, and T_{ST} is the average static torque in the cone, defined from the lumped spring-mass model.

The first part of the piecewise model in equation 4 is defined in Paofini [14] as the viscous contact torque in the cone clutch. The second component is the cone clutch torque which can be found in Socin and Walters [5]. For this work, however, the model includes a static friction torque with estimation for the average torque in the locked cone, parts 3 and 4 of eq. 4; providing a fully defined piecewise friction model for a synchroniser cone clutch that includes an algorithm to identify stick-slip in the cone clutch. Further information on stick-slip models for clutches can be found in Ref. [15].

Chamfer torque, also referred to as indexing or blocking torque, depending on the context is:

$$T_B = F_S R_I \frac{1 - f_I \tan\phi}{f_I + \tan\phi} \quad (5)$$

T_B is the blocking (indexing) torque, R_I is the pitch radius of chamfers, ϕ is chamfer angle, f_I is chamfer friction coefficient. A more fully developed chamfer model during hub indexing must include the direction change if the sleeve is moving forwards or backwards, influencing the friction torque, see Hoshino [2] for details, and maintain the direction of torque based on the chamfer flank contact.

The sleeve position, relative speed at the cone, and alignment of chamfers are all variables that define the torque applied by the synchroniser. Depending on these variables cone clutch torque, chamfer torque, or no torque load is generated by the mechanism. Drawing on the synchronisation process described in Section 2.1 it is now possible to identify when each of these torque in eqs. (4) and (5) should be applied to the model. For example with the sleeve in contact with the blocking chamfers and relative speed in the cone clutch dynamic cone torque is present, eq. (4) part 2, or if slip reduces to zero this reverts to chamfer torque, eq. 5.

2.4. Sleeve modelling

Modelling of the sleeve combines the free motion of the mechanism during the initial and secondary displacement periods, where the hydraulic piston pressure forces the sleeve forward and restrictions are included for seal losses, oil squeezing, and friction losses. Initial sleeve displacement, expanding the resistance component for equation (3):

$$m_S \ddot{x}_S = P_{C1} A_P - P_{C2} A_P - F_D - F_F - F_L \tag{6}$$

Similarly expanding (3) during displacement to contact with the hub:

$$m_S \ddot{x}_S = P_{C1} A_P - P_{C2} A_P - f_R \frac{T_{ST}}{R_I} - F_L \quad (7)$$

Where m_s is sleeve mass, $\ddot{x}_S$ sleeve acceleration, f_R is friction coefficient as sleeve slides over the ring, F_L is seel drag force, F_F is fluid film squeezing force, and F_D is the detent force in Ref. [16].

During ring unblocking and hub indexing the sleeve displacement is constricted by the relative rotation of chamfers, that is, the re-alignment of chamfers to the neutral position releases the sleeve and allows continuation of motion. Using this method for determining sleeve position and velocity as opposed the application of force balance equations is important for capturing the effect of relative vibration of sleeve and gear hub during these two phases of re-alignment.

3. Powertrain lumped model formulation

The development of a model of powertrain equipped with a dual clutch transmission is presented in this section. It follows the basic principles of torsional lumped inertia models that can be found in texts such as Rao [17]. To capture the basic the responses of a vehicle to torsional transients a minimum of four degrees of freedom is required, capturing the lowest vibration modes. For broader frequency ranges multi-body formulation in this paper uses 15DOF with the synchroniser open, and 14DOF when closed, based on the structure in fig. 4 it provides sufficient detail of the main characteristics of the powertrain.

The model includes elements for engine, flywheel, and clutch drum, the simplified transmission model includes coupled wet clutches and simplified gearing with idling components lumped at gears or synchronisers, and allows output via a final drive gear attached to the propeller shaft, transmitting torque to the differential, thence to the hub, and vehicle inertias. Consolidating the 23 inertia elements in Fig. 4, characteristics of the powertrain are considered both in general and during the synchronisation process. Engaged clutches and synchronisers eliminate two elements and gear pairs are reduced to single elements assuming there is no backlash. To finalise the model it is also assumed that the drive shafts, hubs, and vehicle inertias are symmetrical, and therefore can be paired together in doubled stiffness and inertia elements.

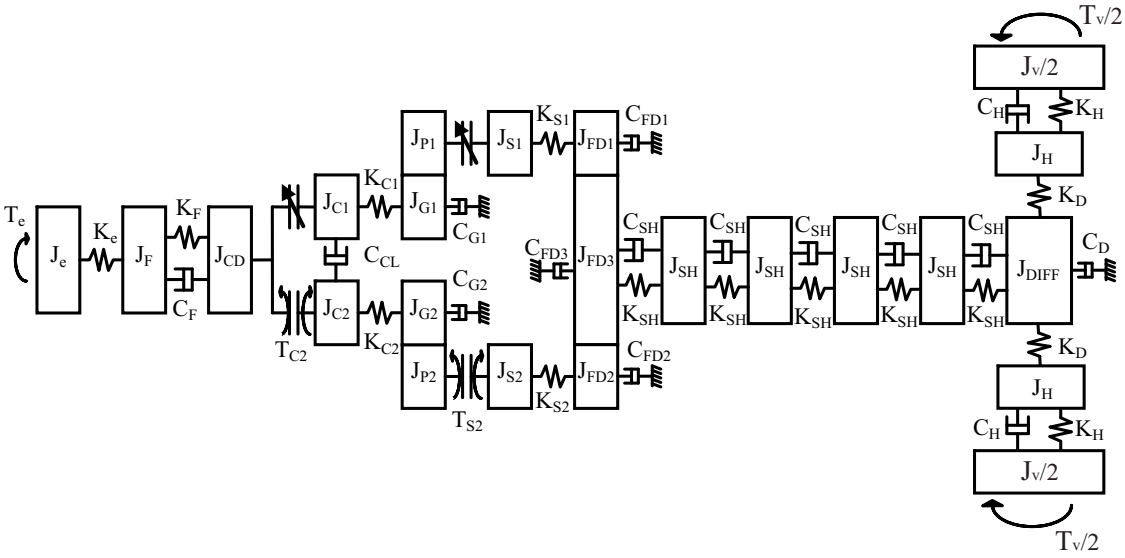

Figure 4: Lumped spring-mass model of a 14 degree of freedom powertrain model

3.1. Model parameters

Model parameters, presented in Table 1, are sourced from know data regarding the DCT or estimated based on published literature. For example, inertia of gears, pinions and synchronisers is determined from available dimensions such as the pitch radius of the gear and mass. In the case of shafts with multiple idling components are present on these shafts, these are lumped as single inertias at gears or synchronisers of interest. For stiffness element measured shaft dimensions are utilised when available, and torsional rigidity calculated using stress-strain relationships.

Damping coefficients represent various forms of loss in the powertrain, such as windage and friction losses in gears or bearings. These are more difficult to determine, generally requiring some form of experimental evaluation to determine. Alternatively, literature evaluating losses in different components of transmission available to estimate losses from these sources, see Changenet, et al, [18] as an example. Alternatively, wet clutch damping, C_{WC}, originates from viscous drag between closely spaced clutch plates, which is investigated by Yuan [19], this solution method is solved over a reasonable speed range and results linearised against relative velocity to determine coefficient C_{WC}. As such damping coefficients must be considered as general losses typical to the powertrain, not as precise data relative to a particular dual clutch transmission design.

Table1: Lumped inertia model parameters

Parameter	Description	Inertia (kg-m^2)	Parameter	Damping (Nms/rad)
J_e	Engine	0.4	C_F	2
J_F	Flywheel	0.2	C_{WC}	0.049
J_{CD}	Clutch drum	0.2	C_{G1}	0.0044
J_{C1}	Clutch pack 1	0.0072	C_{G2}	0.0052
J_{G1}	Gear 1	0.005	C_{FD1}	0.01
J_{P1}	Pinion 1	0.0006	C_{FD2}	0.023
J_{S1}	Synchroniser 1	0.0145	C_{DIFF}	0.1
J_{C2}	Clutch pack 2	0.0125	C_{SH}	0.25
J_{G2}	Gear 2	0.005	C_T	4
J_{P2}	Pinion 2	0.0013	**Parameter**	**Stiffness (Nm/rad)**
J_{S2}	Synchroniser 2	0.0094	K_e	95000
J_{FD1}	Final drive 1	0.0028	K_{DM}	200000
J_{FD2}	Final drive 2	0.0009	K_{C1}	210000
J_{FD3}	Final drive 3	0.16	K_{S1}	560000
$J_{SH\#}$	¼ propeller shaft	0.0007	K_{C2}	870000
J_{DIFF}	Differential	0.16	K_{S2}	470000
J_H	Hub	0.6992	K_{FD3}	165000
J_T	Vehicle + tyre	67.5585	K_{SH}, K_{AX}	165000
-		-	K_T	20000

3.2. Matrix model derivations

The matrix form of Newton's second law as applied to the torsional lumped spring-mass system is prescribed thus:

$$\mathbf{J}\ddot{\boldsymbol{\theta}} - \mathbf{C}\dot{\boldsymbol{\theta}} - \mathbf{K}\boldsymbol{\theta} = \mathbf{T} \tag{8}$$

Where **J** is the inertia matrix in Kg-m^2, **C** is the damping matrix in Nm-s/rad, **K** is the stiffness matrix in Nm/rad, T is the torque vector in Nm, and $\boldsymbol{\theta}$ is rotational displacement in rad, $\dot{\boldsymbol{\theta}}$ is velocity in rad/s and $\ddot{\boldsymbol{\theta}}$ is acceleration in rad/s^2. Off diagonal terms present as negative values to produce an mathematically stable model, and zeros have been omitted from matrices for clarity.

The diagonal inertia element matrix is:

$$\mathbf{J} = \left[J_e \quad J_F \quad \left(J_{CD} + J_{C1}\right) \quad \left(\gamma_1^2 \left(J_{S1} + J_{P1}\right) + J_{G1}\right) \quad J_{C2} \quad \left(J_{G2} + \gamma_2^2 \left(J_{P2}\right)\right) \quad J_{S2} \quad \left(\gamma_{FD1}^2 J_{FD1} + \gamma_{FD2}^2 J_{FD2} + J_{FD3}\right) \quad J_{SH} \quad J_{SH} \quad J_{SH} \quad J_{SH} \quad J_{DIFF} \quad 2J_H \quad \left(2J_T + J_V\right) \right]^{diag}$$

Damping matrix:

$$\mathbf{C} = \begin{bmatrix}
0 & & & & & & & & & & & & & & \\
 & C_F & -C_F & & & & & & & & & & & & \\
 & -C_F & C_F + C_{CL} & -C_{CL} & & & & & & & & & & & \\
 & & & C_{D1} & & & & & & & & & & & \\
 & & -C_{CL} & & C_{CL} & & & & & & & & & & \\
 & & & & & C_{D2} & & & & & & & & & \\
 & & & & & & 0 & & & & & & & & \\
 & & & & & & & \left(\gamma_{FD1}{}^2 C_{FD1} + \gamma_{FD2}{}^2 C_{FD2} + C_{FD3} + C_{SH}\right) & -C_{SH} & & & & & & \\
 & & & & & & & -C_{SH} & 2C_{SH} & -C_{SH} & & & & & \\
 & & & & & & & & -C_{SH} & 2C_{SH} & -C_{SH} & & & & \\
 & & & & & & & & & -C_{SH} & 2C_{SH} & -C_{SH} & & & \\
 & & & & & & & & & & -C_{SH} & C_{SH} + C_D & & & \\
 & & & & & & & & & & & & 0 & & \\
 & & & & & & & & & & & & & 2C_H & -2C_H \\
 & & & & & & & & & & & & & -2C_H & 2C_H
\end{bmatrix}$$

Stiffness matrix:

$$\mathbf{K} = \begin{bmatrix}
K_e & -K_e & & & & & & & & & & & & & \\
-K_e & (K_e + K_F) & -K_F & & & & & & & & & & & & \\
 & -K_F & (K_F + K_{C1}) & -K_{C1} & & & & & & & & & & & \\
 & & -K_{C1} & \left(K_{C1} + \gamma_1^{\,2} K_{S1}\right) & & & & \dfrac{-\gamma_{FD1} K_{S1}}{\gamma_1} & & & & & & & \\
 & & & & K_{C2} & -K_{C2} & & & & & & & & & \\
 & & & & -K_{C2} & K_{C2} & & & & & & & & & \\
 & & & & & & K_{S2} & -\gamma_{FD2} K_{S2} & & & & & & & \\
 & & & \dfrac{-\gamma_{FD1} K_{S1}}{\gamma_1} & & & -\gamma_{FD2} K_{S2} & \left(\gamma_{FD1}{}^2 K_{S1} + \gamma_{FD2}{}^2 K_{S2} + K_{FD3}\right) & -K_{FD3} & & & & & & \\
 & & & & & & & -K_{FD3} & (K_{FD3} + K_{SH}) & -K_{SH} & & & & & \\
 & & & & & & & & -K_{SH} & 2K_{SH} & -K_{SH} & & & & \\
 & & & & & & & & -K_{SH} & 2K_{SH} & -K_{SH} & & & & \\
 & & & & & & & & & -K_{SH} & 2K_{SH} & -K_{SH} & & & \\
 & & & & & & & & & & -K_{SH} & (K_{SH} + K_D) & -K_D & & \\
 & & & & & & & & & & & -K_D & 2(K_D + K_H) & -2K_H & \\
 & & & & & & & & & & & & -2K_H & 2K_H &
\end{bmatrix}$$

Displacement vector, of which the two time derivatives make up the velocity and acceleration vectors:

$$\boldsymbol{\theta} = \begin{bmatrix} \theta_e & \theta_F & \theta_D & \theta_{G1} & \theta_{C2} & \theta_{G2} & \theta_{S2} & \theta_{FD3} & \theta_{SH1} & \theta_{SH2} & \theta_{SH3} & \theta_{SH4} & \theta_{DIF} & \theta_H & \theta_V \end{bmatrix}^T$$

And, torque vector:

$$\mathbf{T} = \begin{bmatrix} T_e & 0 & 0 & -T_{C2} & T_{C2} & -\gamma_2 T_{S2} & T_{S2} & 0 & 0 & 0 & 0 & 0 & 0 & 0 & -T_V \end{bmatrix}^T$$

3.3. Clutch torque model

The applied clutch torque, T_{C2}, would typically be included as a piecewise linear model, see Crowther [20] as an example. Clutch torque is defined using three states, (1) open with the applied forced, friction coefficient and clutch geometry determining the clutch torque, (2) closed where the clutch torque is an average torque derived from acceleration of inertia and element stiffness's, this is limited by state (3), the static friction limit of the closed clutch. For the purpose of these simulations there is no load on the clutch and torque is maintained at zero.

3.4. Engine torque models

Two separate engine models will be employed in these simulations. The mean engine torque (Fig. 5 (a)) derived from a lookup table relating engine torque to speed and percent throttle, in this model constant throttle is maintained, thus engine torque varies as a function of speed.

The second model is used to analyse the influence of engine torque harmonics on the powertrain, simulating the torque variation from piston firing. See Fig. 5 (b) showing output engine torque over two shaft revolutions, or one cycle of a four stroke engine. Using the method set out in Taylor [21] the variation of piston head pressure, crank angle, inertia of connecting rods, crank shaft and piston are used to generate engine torque that varies with crank angle, with a mean torque of 326Nm.

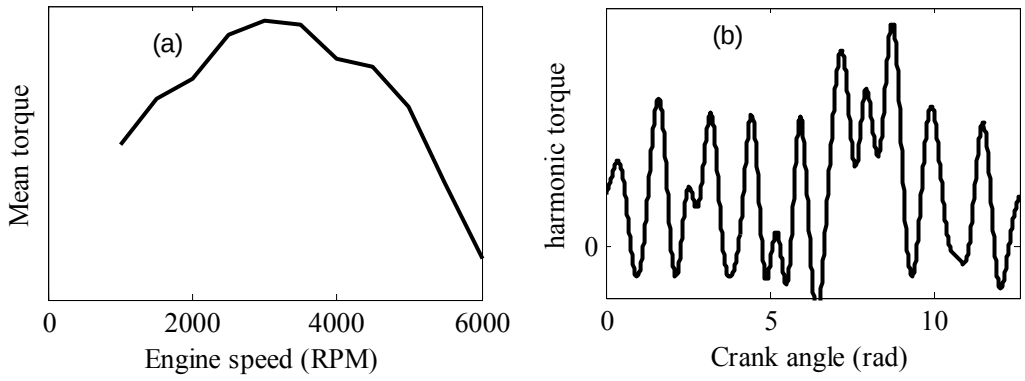

Figure 5: Engine torque maps for simulations, (a) mean torque model map, and (b) transient engine torque model map

3.5. Vehicle resistance torques

Vehicle resistance torque comprises of vehicle drag, rolling resistance and incline loads. With a road angle of zero degrees this incline load can be excluded, the vehicle resistance torque is:

$$T_V = \left(\frac{1}{2} \rho_{air} A_v C_D V^2 + M_v g C_T \right) \times R_W \qquad (9)$$

Where $M_{v\,is}$ vehicle mass, A_v is vehicle area, C_D is drag coefficient, V is vehicle speed, ρ_{air} is air density, and C_T tire rolling resistance coefficient.

4. Damped free vibration analysis

To demonstrate the adequacy of this model the first results presented are for the natural frequencies and corresponding damping ratios of the powertrain model before and after synchronisation. Applying the Eigenvalue problem to the system matrix complex damped natural frequency pairs are returned as Eigenvalues, see Rao [17] for detailed

description of method. From these results the natural frequencies and damping ratios are obtained for both system states.

Table 2: Powertrain natural frequency and damping ratios for fourth gear frewheeling and synchronised in the powertrain

Powertrain state:	*3rd gear engaged, 4th gear freewheeling*		*3rd gear engaged, 4th gear synchronised*	
	ω_n (Hz)	ζ (%)	ω_n (Hz)	ζ (%)
1	RBM	-	RBM	-
2	RBM	-	-	-
3	6	0.26	6	0.2
4	34	1.26	34	1.26
5	99	0.07	98	0.06
6	229	0.19	225	0.44
7	233	0.48	231	0.15
8	429	0.06	325	0.16
9	1027	0.01	737	0.01
10	1563	0.99	1274	0.02
11	1788	0.02	1569	0.99
12	1965	0.01	1926	0.01
13	2970	1.78	2970	1.78
14	4085	2.21	4085	2.21

15	4801	2.37	4801	2.37

Referring to Table 2, the lowest natural frequency, 0 Hz, is the rigid body mode (RBM) of the system, with the 4th gear freewheeling there are two rigid body modes present in the open synchroniser model, one for the powertrain and the other for the freewheeling gears targeted for synchronisation. While with the synchroniser closed there is only one rigid body mode for the entire system. Natural frequencies of 6, 34 and 98 Hz are consistent with shuffle, hub and clutch drum vibration models. The Eigen value solutions produced 13 negative paired solutions for both open and closed synchroniser powertrains, with the other solutions being for the rigid body modes as previously discussed, consisting of very small values (10^{-13}) signifying numerical error. These results demonstrate that this is a semi definite system, in that it is not physically constrained, including the freewheeling synchroniser in the powertrain for the open synchroniser model, and, more importantly, indicate that powertrain is stable for both open and closed states.

The direct result of locking the synchroniser is to eliminate one degree of freedom in the powertrain model, and alter the local inertia in the transmission. Observed from table one is the modification of local natural frequencies 8 through to 11 as a direct result of synchroniser lockup and increase in local inertia. As the structure of system damping is not modified significantly it can be concluded that ω_{n11} in the open model is reduced below that of ω_{n10} rather than both natural frequencies being reduced in the closed synchroniser free vibration results.

5. Synchroniser engagement simulations

5.1. Transient simulations with ideal engine torque model

The powertrain model was built up in the Matlab environment with open and closed synchroniser models. Synchroniser engagement simulations were performed using the ODE45 from the ODE suite with a maximum time step of 10^{-5} for the powertrain model, and a time step of 10^{-7} for the hydraulic control model, relative tolerance is set to 10^{-4} and absolute tolerance 10^{-7}. The use of two simulation time steps significantly reduces computational requirements when the hydraulic system is not active. Event functions were used to determine lockup conditions and move between powertrain models.

The first series of simulations use the ideal engine model to simulate the mechanism engagement without interference from the engine torque harmonics. For initial simulations a general shift case for a fourth gear synchronisation with third gear engaged is considered. For these conditions the initial wheel speed is set to 40 rad/s with a corresponding engine speed of 182 rad/s, and throttle angle at 50%.

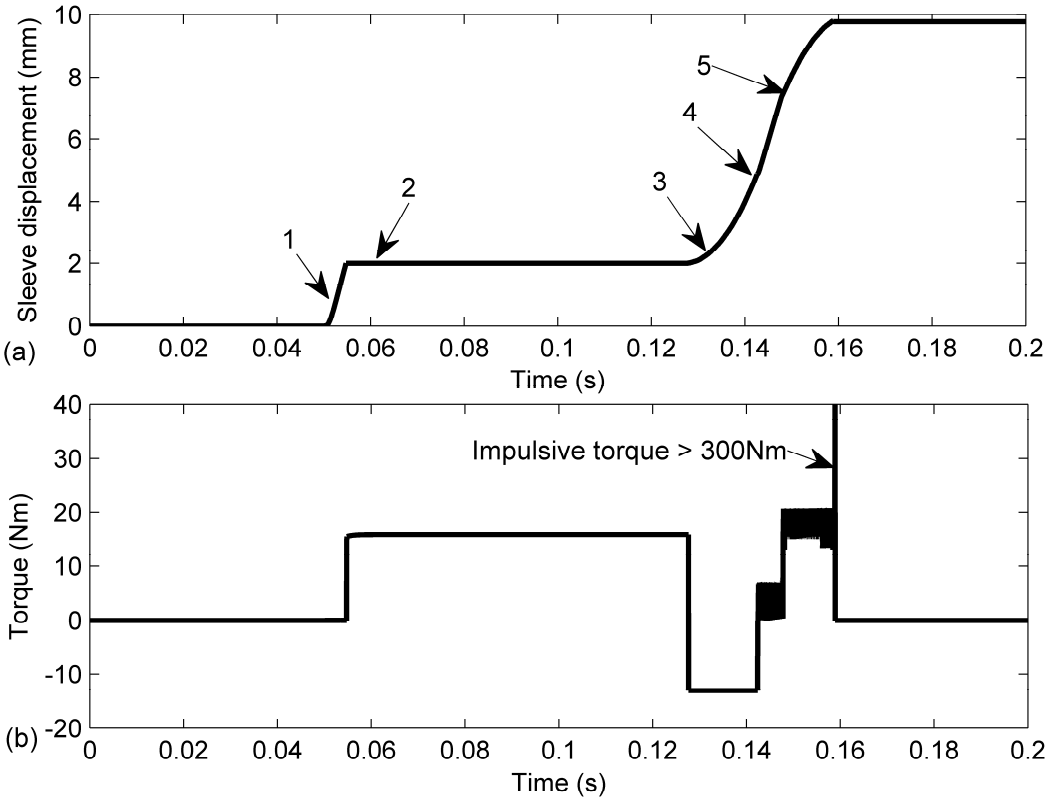

Figure 6: Synchroniser engagement responses, showing (a) sleeve displacement during engagement and, (b) effective synchroniser torque

Sleeve displacement and torque developed during the mechanism engagement are presented in Fig. 6. At 50ms the synchroniser is actuated and moves forward rapidly as hydraulic pressure increases, with the initial displacement taking less than 5ms, at 1. At arrow 2 speed synchronisation is performed using cone clutch torque, while the sleeve remains stationary. With the components synchronised the sleeve moves forward again and the torque rapidly changes direction as blocking chamfers now take up the primary torque role at arrow 3, the reversal of torque demonstrating the torque balance between piecewise cone model and blocking chamfers during synchronisation. The sleeve pushes forward until it breaches the ring chamfers, the cone is released at approximately 140ms

and the sleeve moves forward freely, see arrow 4. The unsteady torque here results from vibration in sleeve and gear generating a changing friction load on the cone clutch as the sleeve slides over the ring. There is then the final chamfer torque as the hub is indexed with the sleeve and interlocks the mechanism at arrow 5. This engagement is slowed by resistances acting against the chamfer torque with vibration of the sleeve again causing oscillations in the chamfer torque at frequency 1788Hz, the local natural frequency for the freewheeling components with low inertia and higher shaft stiffness prior to lockup of the synchroniser, see free vibration analysis results.

As the sleeve completes the engagement there is still a relative speed between the two elements. With lockup a torque impulse is generated in the sleeve as a restitution load to halt any remaining relative motion. Though over 300Nm this torque is developed numerically and is heavily dependent on the time step used during the simulation. Overall the synchroniser torque can be characterised as being highly nonlinear and heavily dependent on sleeve position and relative speed between hub and sleeve.

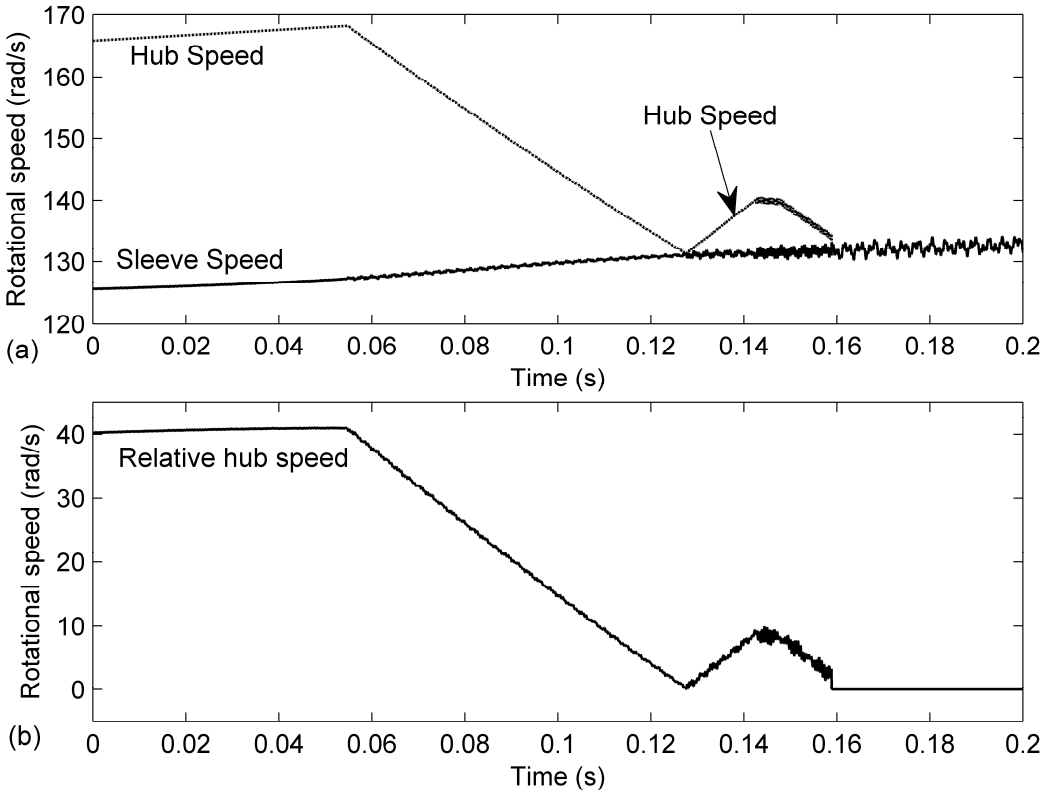

Figure 7: Synchroniser hub and sleeve speeds (a), and synchroniser relative speed (b)

In Fig. 7 the absolute and slip speed results for sleeve and hub of the target gear are presented for the duration of the process. With high viscous drag in the wet clutch the speed of the target gear is actually higher than that of the sleeve when synchronising a higher gear. At end of blocking the impulse created through realignment of the ring as it is captured by the sleeve breaks the cone lock and significant slip speed is introduced to the mechanism before indexing of the mechanism. This can be an issue as high slip speeds during chamfer contact at hub indexing can also lead to impact damage with chamfer teeth. This results in increased vibration during indexing of the hub and target gear that is not experienced during unblocking of the ring. These are similar processes but the ring unblocking begins with a zero relative velocity. At end of indexing the

trapping of hub inside sleeve produces a step speed changed consistent with the lockup shock torque discussed previously. This step change, in conjunction with the inertia change, is the primary reasons behind significant post lockup vibration of the mechanism. Another critical aspect of this simulation is the identification of stick-slip in cone clutch at end of synchronisation and before unblocking of the ring. Fig. 8 provides evidentiary demonstration of minimal stick-slip upon lockup of the cone clutch, unblocking of the ring then commences rapidly. This provides minimal delay to the process of engagement at the beginning of unblocking the ring.

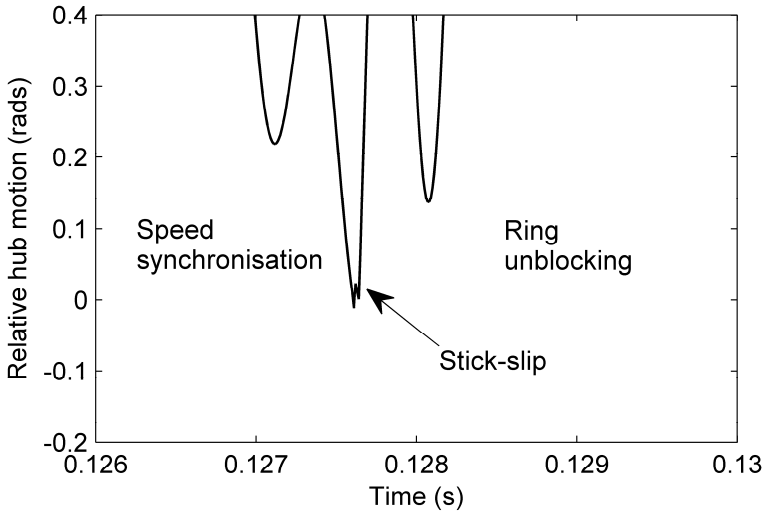

Figure 8: Synchroniser relative speed demonstrating stick - slip during final stages of speed synchronisation before clutch lockup

5.2. Transient simulations with engine harmonic torque model

To study the effect of torque variation from engine harmonics on the synchronisation process the piston firing engine model described in Section 3.4 is applied to the

powertrain model and simulations performed using the same parameters and initial conditions set out in Section 5.1.

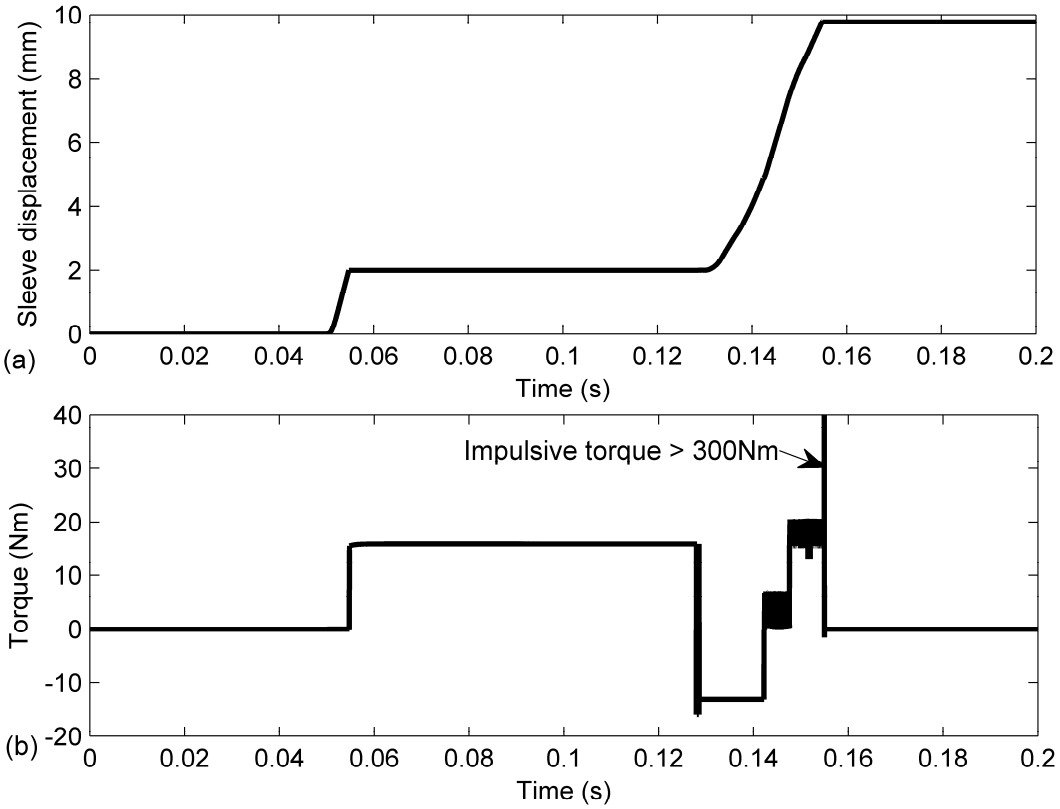

Figure 9: Synchroniser engagement responses using dynamic engine model, showing (a) sleeve displacement during engagement and, (b) effective synchroniser torque

Comparatively speaking results for Figs. 6 and 9 are very similar, however, at the end of synchronisation there is evidence of stick-slip phenomena in the cone clutch. Sleeve displacements are consistent, and the duration of engagement does not change significantly. The fluctuation of chamfer torque during indexing is again present, noting that such vibrations may contribute to increased wear on chamfer contact surfaces, reducing effectiveness of the chamfer engagement during the indexing of the mechanism.

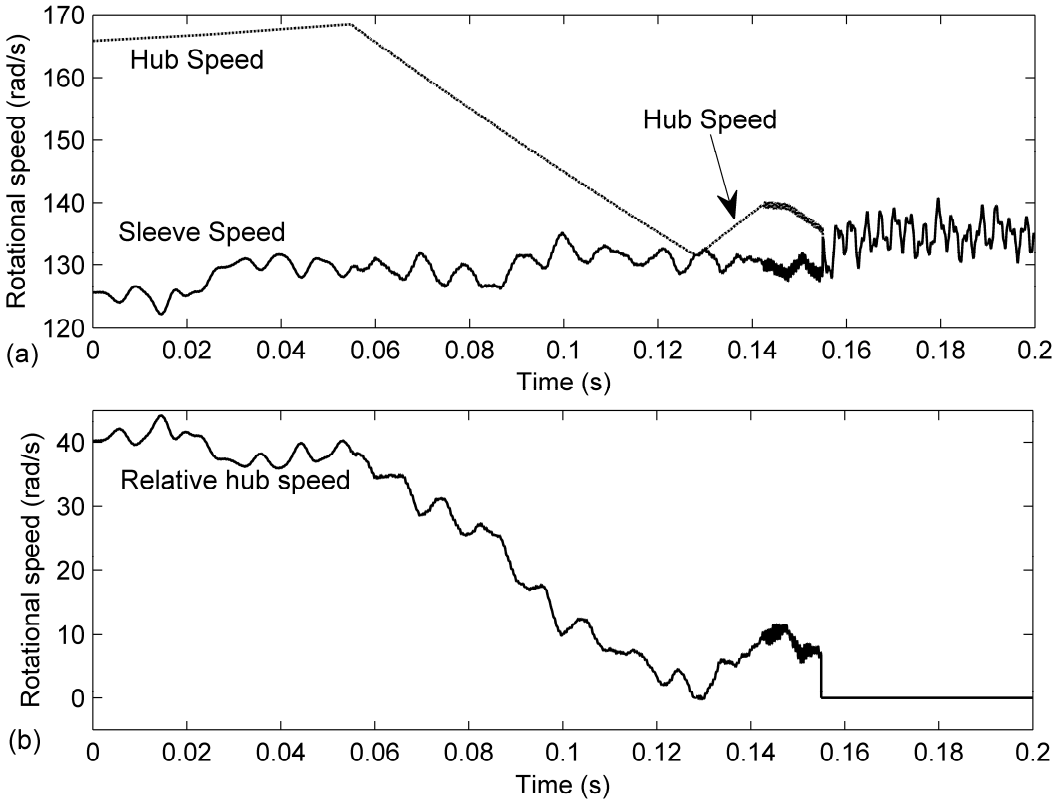

Figure 10: Synchroniser hub and sleeve speeds (a), and synchroniser relative speed (b) using dynamic engine model

The effects of introducing engine torque harmonics onto the powertrain are significantly more pronounced in the synchroniser sleeve and hub rotational speeds. During the initial steady state period sleeve vibration has increased considerably, reflected in the cone slip speed. However, with the exception of indexing, the engagement process is reasonably similar to Fig. 7. During indexing there is increased vibration of the sleeve in particular. This must be considered a negative influence of engine torque harmonics on the engagement of the mechanism, and again is likely to contribute to increased wear of chamfer contact surfaces. Stick slip periods are present in the mechanism post speed synchronisation and are significantly pronounced, shown in Fig. 11. In Fig. 8 there is

only minor evidence of stick-slip occurring, however, with engine vibration, there is increased stick slip that restricts initiation of unblocking of the synchroniser mechanism.

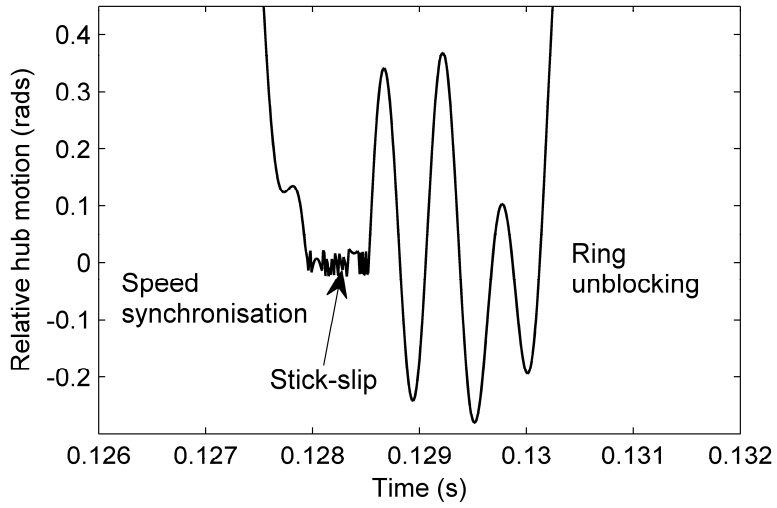

Figure 11: Demonstration of stick-slip phenomena using a dynamic engine model

6. Comparison of responses during synchronisation for mean and harmonic engine torque models

To further investigate the influence of wear on the mechanism through the introduction of engine harmonics, comparison of sleeve relative vibration during both synchronisation and indexing of the mechanism is performed. The results are presented in Fig. 12, and Fast Fourier Transforms of a discrete system is preformed for the synchroniser open period to identify the introduction of forced engine vibrations. Given the torques acting on the synchroniser sleeve in Figs. 6 and 9 are positive, negative amplitude vibrations are more likely to contribute to the early unblocking of the mechanism as these are likely to aid release of the chamfers.

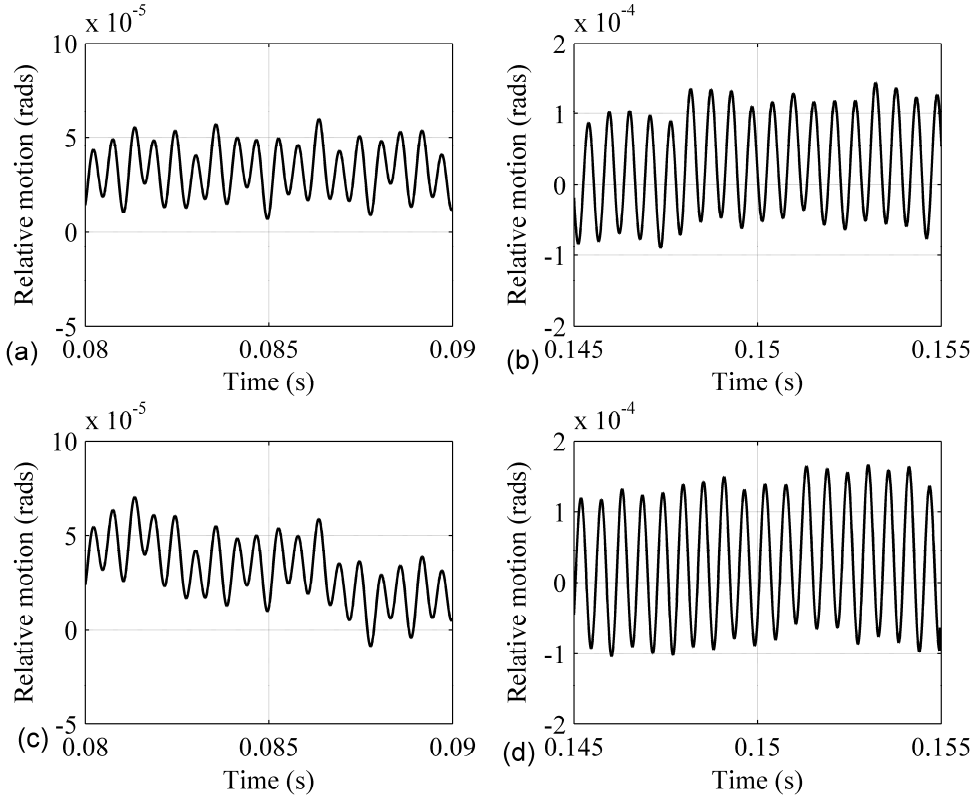

Figure 12: Relative vibration synchroniser sleeve during actuation of the synchroniser mechanism. For the ideal engine models (a) during synchronisation and (b) during indexing, and using the engine harmonic torque model (c) during synchronisation and (d) during indexing

Fig. 12 demonstrates the relative vibration amplitudes of the synchroniser sleeve during different stages of engagement. During synchronisation, Fig. 12 (a) and (c), vibrations are reasonably consistent with similar vibration amplitudes but a low order frequency can be observed in the harmonic torque model. The results for engine vibrations suggests the possibility for negative vibrations, however this is only for small periods. Thus, while there are negative vibrations present these are unlikely to be sufficient to cause early unblocking of the synchroniser ring.

In the graphics Fig. 12 (b) and (d) the response during indexing with engine harmonics included a significant increase in vibration in addition to results using mean engine torque. This is consistent with earlier demonstrated results, in that the introduction of the engine model contributes to increased vibration of synchroniser components during indexing in particular, suggesting that there is the likelihood of increased wear on the chamfer contact surfaces.

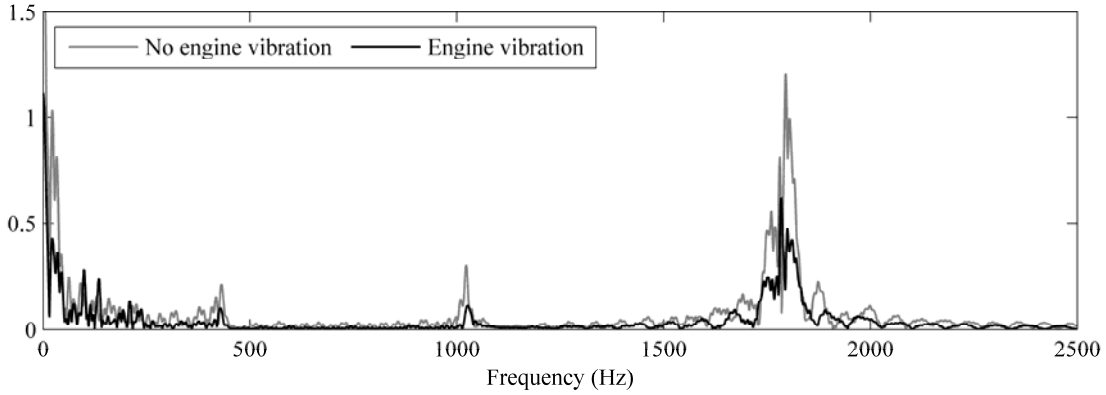

Figure 13: Fast Fourier Transforms of sleeve relative vibration during synchronisation

A more extensive result of the influence of engine vibration can be observed using Fast Fourier Transforms of the sleeve relative vibration during the period with the synchroniser energised. With no engine vibration the influence of system natural frequencies is much more dominant on the powertrain, with peaks corresponding to $\omega_{n8,}$ $\omega_{n9,\ and}$ ω_{n11} in Table 2. These natural frequencies are observed in the FFT results for simulations with engine vibration as well, but are less dominant that the ideal model. However at low frequencies, those below 500Hz, much of these results are hidden by noise generated by numerical error associated with using Fourier transforms on a discrete data set. Fig. 14 provides a scaled up view of the low frequency responses, the peaks

indicated by arrow 1 indicate the frequency responses introduced from engine forced vibration. It must be noted that the engine vibration is a forced vibration dependent on the engine speed, insofar that the frequency response is dependent on speed and frequencies increase with engine acceleration. The introduced forced vibration is observed in Fig. 10 with external oscillations superimposed over the synchroniser response in Fig. 7, with only a mean torque engine model applied.

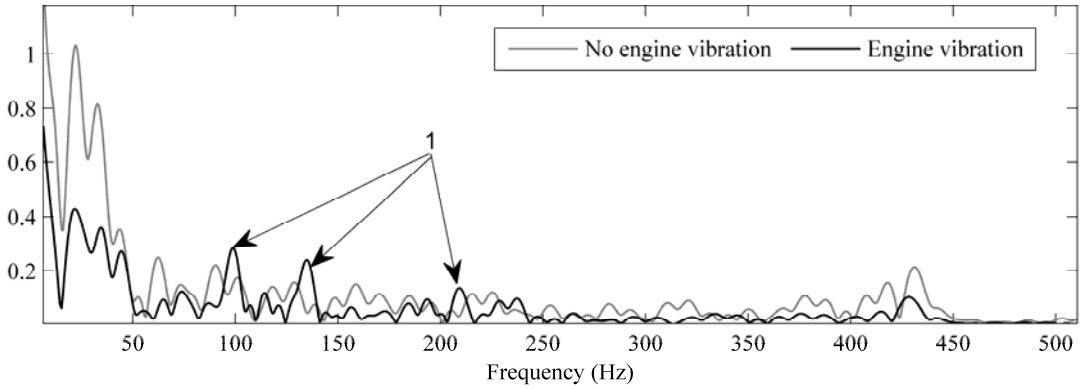

Figure 14: Enlarged view of FFT results in figure 12, focus on frequencies less than 500Hz

7. Conclusion

A 15DOF lumped spring-mass powertrain model for the investigation of synchroniser mechanism engagement in a dual clutch transmission has been developed in this paper for the analysis of synchroniser engagement. This includes the integration of hydraulic control system, a piecewise nonlinear synchroniser model that incorporates torques from both cone clutch and control chamfers, and engine models using mean torque and harmonic torques from piston firing. These were applied to investigate the engagement dynamics of the synchroniser mechanism in a powertrain equipped with a DCT. Speed

synchronisation, ring unblocking and indexing of the mechanism were all demonstrated to be effective using the mean torque engine model. It was shown that the impulsive speed change between sleeve and ring upon completion of unblocking generates sufficient torque to release the locked cone clutch, resulting in a relative speed between sleeve and hub chamfers before indexing, resulting in increased vibration during indexing.

The introduction of engine torque harmonics to the system was performed to demonstrate the transmissibility of vibrations to the synchroniser and its influence on engagement. The development of stick-slip in the cone prior to unblocking was identified in the later stages of speed synchronisation, resulting from the higher torsional vibration in the system. Increased vibration was also present during indexing, with more substantial response than demonstrated in the mean torque simulations.

Results were expanded to include the study of relative motion on the sleeve, and its potential increase with the engine torque harmonics. Overall these results have demonstrated that engine vibration may contribute to increase the increased vibration in the synchroniser mechanism, which is likely to increase wear on the mechanism, most notably on indexing chamfers where degradation of contact surfaces are likely to inhibit the correct actuation and engagement of the synchroniser. Additionally there is also the present of small negative torques in the sleeve as a result of higher vibrations during speed synchronisation. Though present these are not sufficient to cause early unblocking of the ring for the conditions present in this simulations, but must be considered

important if detrimental engagement conditions are present, such as poor oil wiping of cone friction surfaces or excessive drag.

Appendix A

To develop the pressure model of the two hydraulic cylinders presented in Fig.3, begin with the differentia1 equation of a compressible fluid:

$$Q = \frac{V}{\beta}\frac{dP}{dt} \tag{A.1}$$

Arranged to make pressure the subject

$$\int dP = \int \frac{Q \cdot \beta}{V} dt \tag{A.2}$$

With motion of the sleeve the volume of the cylinder will change, thus volume is not constant, or:

$$\int dP = \int \frac{Q \cdot \beta}{V_0 + dV} dt \tag{A.3}$$

It is assumed that the bulk modulus, β, is constant, so the relevant flow rates are required for inflow from the orifice, rate of change of cylinder, and leak flow out of the control volume. Q is therefore:

$$Q = Q_{Orifice} + Q_{Volume} + Q_{Leak} \tag{A.4}$$

Or, based on equations for sharp edged orifice and annular orifice presented in [22], and the rate of change in volume of the cylinder:

$$Q = C_D \pi \frac{D_{CV1}^{\ 2}}{4} \sqrt{P_{Syn} - P_{C1}} - A_P \frac{dX_S}{dt} - C_D \pi D_S c_r \sqrt{P_{C1} - P_{Exh}} \tag{A.5}$$

Equation A.5 is then substituted into equation A.3 to give eqs. 1 and 2, repeated below, note that the sign difference for the volume rate of change is required as the piston heads move in opposing directions for the two cylinders:

$$P_{C1} = \int \frac{\beta}{V_0 + dV}\left(C_D \pi \frac{D_C{}^2}{4}\sqrt{P_{syn} - P_{C1}} - A_P \frac{dX_{syn}}{dt} - C_D \pi D_C c_r \sqrt{P_{C1} - P_{Exh}} \right) dt \qquad \text{(A.6)}$$

References

[1] D Kelly, C Kent, Gear shift quality improvement in manual transmissions using dynamic modelling, *FISITA 2000 World Automotive Congress*, Seoul Korea, June 2000, paper number: F2000A126.

[2] H Hoshino, Analysis on synchronisation mechanism of transmission, *SAE World Congress & Exhibition, Session: Transmission and Driveline Systems*, Detroit, Michigan, April 1999, paper number: 1999-01-0734.

[3] Y Liu, C Tseng. Simulation and analysis of synchronisation and engagement on manual transmission gearbox, *International Journal of Vehicle Design,* 43 (2007) 200-220.

[4] L Lovas, D Play, J Marialigeti, J Rigal. Mechanical behaviour simulation for synchromesh mechanism improvements, *Proceeding of the Institution of Mechanical Engineers Part D: J Automobile Engineering*, 220 (2006) 919-945.

[5] RJ Socin, LK Walters. Manual transmission synchronizers, *SAE technical paper series*, paper number: 680008.

[6] E M'Ewen. The theory of gear changing, *Proceedings of the Institution of Mechanical Engineers* (1948) 30-40.

[7] AR Crowther, R Singh, N Zhang, C Chapman. Impulsive response of an automated transmission system with multiple clearances: formulation, simulation, and experiment, *Journal of Sound and Vibration* 306 (2007) 444-466.

[8] N Zhang, A Crowther, DK Liu, J Jeyakumaran. A lumped spring-mass method for the dynamic analysis of automatic transmission gear shifting with a four-degree-of-freedom planetary gearset element, *Proceedings of the Institution of Mechanical Engineers Part D: J Automobile Engineering* 217 (2003) 461-473.

[9] M Goetz, Integrated powertrain control for twin clutch transmissions, PhD Thesis, University of Leeds, 2005.

[10] S Kirschstein. The impact of launch control on the vibration behaviour of a dual clutch transmission powertrain, *VDI Berichte* 1971 (2007) 197-217.

[11] M Goetz, M Levesley, D Crolla. A gearshift controller for twin clutch transmissions, *VDI Berichte* 1786 (2003) 381-400.

[12] PR Crossley, JA Cook , A nonlinear engine model for drivetrain system development, *International conference on control,* Edinburgh, UK, March 1991, 921-925.

[13] M Kulkarni, T Shim, Y Zhang. Shift dynamics and control of dual-clutch transmissions, *Mechanism and Machine Theory* 42 (2007) 168-182.

[14] B Paffoni, R Progri, R Gras, J Blouet. The hydrodynamic phase of gearbox synchromesh operation: the influence of radial and circumferential grooves, *Proceedings of the Institution of Mechanical Engineers: Part J: J Engineering Tribology* 211 (1997) 107-116.

[15] A Crowther, N Zhang, DK Liu, J Jeyakumaran. Analysis and simulation of clutch engagement judder and stick-slip in automotive powertrain systems, *Proceedings of the*

Institution of Mechanical Engineers Part D: J Automobile Engineering 218 (2004) 1427-1446.

[16] ST Razzacki. Synchroniser design: a mathematical and dimensional treatise, *SAE World Congress & Exhibition, Session: Transmission and Driveline Systems*, Detroit, Michigan, March 2004, paper number 2004-01-1230.

[17] S. S. Rao, *Mechanical Vibrations*, 1st ed., Addison-Wesley Publishing Co., Reading USA, 1986.

[18] C Changenet, X Oviedo-Marlot, P Velex. Power loss predictions in geared transmissions using thermal networks-application to a six speed manual gearbox, *Transactions of the American Society of Mechanical Engineers*. 128 (2006) 618-625.

[19] Y Yuan, E Liu, J Hill, Q Zou. An Improved hydrodynamic model for open wet transmission clutches, *Journal of Fluids Engineering*. 129 (2007) 333-337.

[20] A Crowther, N Zhang. Torsional lumped spring-mass and nonlinear modelling in vehicle powertrain dynamics, *Journal of Sound and Vibration* 184 (2005) 825-849.

[21] C F Taylor. *Internal combustion engines in theory and practice: Volume 2: Combustion, fuels, materials, and design*, 2nd ed., MIT Press, USA, pp 240-295.

[22] J. Stringer, *Hydraulic systems analysis, an introduction,* 1st ed., Macmillan Press Ltd., London, UK, 1976.

Figure Captions

Figure 1: Typical synchroniser mechanism cross-section

Figure 2: Chamfer contact positions during separate steps of the synchronisation process, (a) sleeve in neutral position, (b) sleeve and ring in blocking position, (c) sleeve and hub in indexing position, and (d) sleeve interlocked with hub. T_D should be considered the net resistance torque acting on the synchroniser mechanism.

Figure 3: Double acting cylinder model for the actuation of the synchroniser sleeve

Figure 4: Lumped spring-mass model of a 14 degree of freedom powertrain model

Figure 5: Engine torque maps for simulations, (a) mean torque model map, and (b) transient engine torque model map

Figure 6: Synchroniser engagement responses, showing (a) sleeve displacement during engagement and, (b) effective synchroniser torque

Figure 7: (a) Synchroniser hub and sleeve speeds, (b) and synchroniser relative speed

Figure 8: Synchroniser relative speed demonstrating stick - slip during final stages of speed synchronisation before clutch lockup

Figure 9: Synchroniser engagement responses using dynamic engine model, showing (a) sleeve displacement during engagement and, (b) effective synchroniser torque

Figure 10: (a) Synchroniser hub and sleeve speeds, and synchroniser relative speed (b) using dynamic engine model

Figure 11: Demonstration of stick-slip phenomena using a dynamic engine model

Figure 12: Relative vibration synchroniser sleeve during actuation of the synchroniser mechanism. For the ideal engine models (a) during synchronisation and (b) during indexing, and using the engine harmonics model (c) during synchronisation and (d) during indexing

Figure 13: Fast Fourier Transforms of sleeve relative vibration during synchronisation

Figure 14: Enlarged view of FFT results in figure 12, focus on frequencies less than 500Hz

Table Captions

Table 1: Lumped inertia model parameters

Table 2: Powertrain natural frequency and damping ratios for fourth gear frewheeling and synchronised in the powertrain